doi:10.1007/s11589-011-0771-9

Spatial variations of the 660-km discontinuity in the western Pacific subduction zones observed from CEArray triplication data*

Baoshan Wang[1,♦] and Fenglin Niu[2]

[1] *Institute of Geophysics, China Earthquake Administration, Beijing* 100081, *China*
[2] *Department of Earth Science, Rice University, Houston, TX* 77005, *USA*

Abstract We examined the spatial variation of velocity structures around the 660-km discontinuity at the western Pacific subduction zones by waveform modeling of triplication data. Data from two deep earthquakes beneath Izu-Bonin and Northeast China are used. Both events were well recorded by a dense broadband seismic network in China (CEArray). The two events are located at approximately the same distance to the CEArray, yet significant differences are observed in their records: (1) the direct arrivals traveling above the 660-km discontinuity (AB branch) are seen in a different distance extent: ∼29° for the NE China event, ∼23° for Izu-Bonin event; (2) the direct (AB) and the refracted waves at the 660-km (CD branch) cross over at 19.5° and 17° for the NE China and the Izu-Bonin event, respectively. The best fitting model for the NE China event has a broad 660-km discontinuity and a constant high velocity layer upon it; while the Izu-Bonin model differs from the standard IASP91 model only with a high velocity layer above the 660-km discontinuity. Variations in velocity models can be roughly explained by subduction geometry.

Key words: **P-wave triplication; 660-km discontinuity; western Pacific subduction zone**
CLC number: P315.2 **Document code**: A

1 Introduction

The 660-km seismic discontinuity dividing the upper and lower mantle plays a significant role in large-scale mantle circulation (e.g., Tackley, 2008). The seismic discontinuity is generally believed to be caused by the dissolution of γ-olivine or ringwoodite into perovskite plus magnesiowustite (Ito and Takahashi, 1989). In general, the phase transition (also known as the post-spinel transformation) is observed to occur within a relatively narrow pressure range, consistent with a sharp 660-km discontinuity observed seismically. Laboratory experiments also showed that ringwoodite tends to dissolve under higher-pressure and lower-temperature conditions, consistent with depressed 660-km discontinuities seen in cold subduction regions (e.g., Shearer and Masters, 1992; Vidale and Benz, 1992; Niu et al., 2005).

Several receiver function studies (e.g., Niu and Kawakatsu, 1996; Ai et al., 2003; Andrews and Deuss, 2008) indicated that the 660-km discontinuity beneath subduction regions has complicated structure featured by multiple velocity jumps rather than a simply depressed discontinuity. Recently, Wang and Niu (2010) found a broad 600-km discontinuity (velocity increases gradually in a depth range of 50–70 km) beneath NE China with waveform triplication data recorded by a dense broadband seismic network in China. The broadened discontinuity was interpreted to be caused by multiple phase transitions associated with the dissolutions of olivine and garnet within a cold subducted slab. Numerical calculation of mantle velocity (Vacher et al., 1998) also indicated the multiple phase changes could result in a series of velocity jumps in the depth range of ∼660–720 km. The geodynamic implication of such a broad 660-km is, however, not well understood. It is also unclear how pervasive such a broadened 660-

* **Received** 20 September 2010; **accepted in revised form** 22 December 2010; **published** 10 February 2011.
♦ **Corresponding author. e-mail**: wangbs@cea-igp.ac.cn

km discontinuity is present at various sections of the subducting Pacific slab.

The Pacific Plate have been subducting beneath Japan and the Izu-Bonin arc in the last 50 Ma. At the northern section, the Pacific Plate is subducting beneath the Eurasian Plate at a speed ~10 mm/a with a relatively low descending angle. At the southern section, the Pacific Plate is descending at a near vertical angle beneath the Philippine Sea Plate (e.g., Fukao et al., 2001; Nakajima and Hasegawa, 2007). Moderate to large deep focus earthquakes occur within both sections of the subducting Pacific Plate. As the region is relatively well instrumented, it is thus an idea place to study the fine seismic structure at the upper-lower mantle boundary (e.g., Niu and Kawakatsu, 1996; Ai et al., 2003; Tajima et al., 2009; Wang and Chen, 2009).

One of the most frequently used methods in studying the 660-km discontinuity is forward modeling of the wave bifurcation arising from the discontinuity recorded at epicentral distances between ~10° and 30°. The multiple arrivals recorded at a station share very similar ray paths near the source and the receiver sides, thus the differential travel time and relative amplitude among these arrivals are not sensitive to shallow structures. This method has been widely used to study the 660-km discontinuity beneath various subduction zones (e.g., Tajima and Grand, 1998; Brudzinski and Chen, 2003; Wang et al., 2006; Wang and Chen, 2009).

To better monitor seismic activities in China, the China Earthquake Administration (CEA) has upgraded and expanded its national and regional networks over the last decade. Currently, CEA owns one of the largest permanent broadband seismic network in the world, which consists of one national network, 31 regional networks, and several other networks. The networks can be integrated as a large seismic array, which will be referred to as CEArray in the remainder of this paper. CEArray include more than 1 000 stations (Figure 1), among which ~900 are broadband (Zheng et al., 2009). In a recent study, we (Wang and Niu, 2010, hereafter referred to as WN10) analyzed CEArray data from a deep earthquake occurred near the border among China, Russia and North Korea to investigate lateral variations around the 660-km beneath Northeast China. Here we used a similar approach to study the triplication data from a deep earthquake occurring at the Izu-Bonin region. We then compared the velocity structure obtained here with those determined by WN10 to study lateral variations of the 660-km discontinuity.

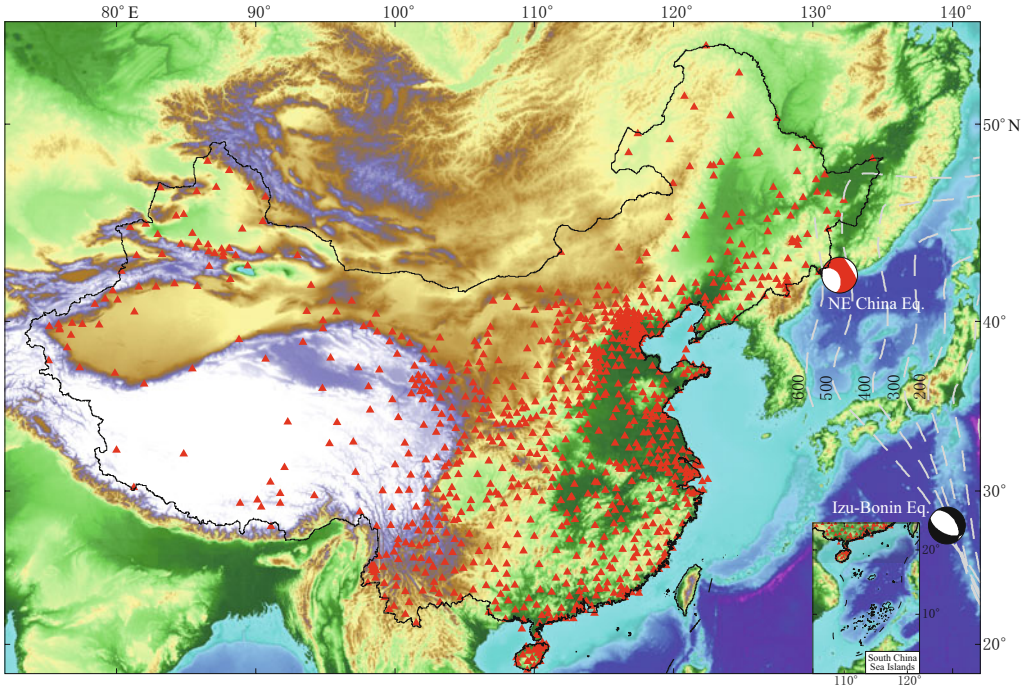

Figure 1 Map showing the stations of the national and regional networks operated by the China Earthquake Administration (solid triangles). Also shown is the focal mechanism of two deep earthquakes used in this study (beach balls). Contours of upper boundary of the subducting Pacific slab are outlined by dashed gray lines.

2 Data and method

A sudden increase of seismic velocity within mantle could result in multiple arrivals of P- and S-waves at a single distance, leading to the so-called waveform triplication. The wave chain includes the direct arrival traveling above the seismic discontinuity, the waves reflected and refracted at the seismic discontinuity. In Figure 2, we showed an example of the ray paths of the three arrivals associated with the 660-km discontinuity, together with their arrival times from a deep earthquake. As shown in Figure 2a, ray paths for direct (AB), reflected (BC), and refracted (CD) waves are quite close to each other at the uppermost mantle and crust. Thus the relative moveouts and amplitude contrast between the direct and refracted phases are very sensitive to velocity structure right above and below the discontinuity (e.g., Tajima and Grand, 1998; Brudzinski and Chen, 2003; Wang et al., 2006; Wang and Chen, 2009; Wang and Niu, 2010).

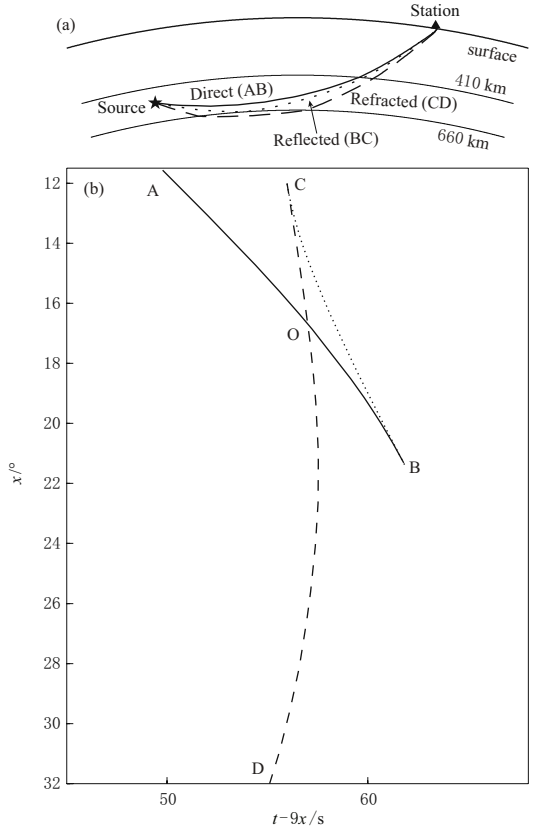

Figure 2 Schematic ray paths of the multiple arrivals (a) and the calculated travel times of these arrivals (b). x denotes the distance, which also have the same meaning in Figures 4, 6, 7. A 520 km deep source and the IASP91 model were used in calculating the travel times. The direct AB phase, the reflected BC phase, and the refracted CD phase are shown in solid, dotted, and dashed lines, respectively.

We found a total of eight earthquakes occurring between 2008 and 2009 with a focal depth >410 km and magnitude >5 within the triplication distances of the CEArray. To analyze the triplication induced by the 660-km discontinuity, we used following criteria to select the events. Events with moderate magnitude are preferred, because they are strong enough to be clearly recorded by most stations and also they usually have simple source time functions. On the other hand, to fully track the triplication we required a full coverage of recordings in the distance range between 10° and 30°. Based on these requirements, we selected two earthquakes for further study.

The first event is located near the border of east Russia and Northeast China, hereafter referred to as NE China event (Figure 1). The NE China event occurred on May 19, 2008 with a focal depth of 520 km and a moment magnitude 5.7 (Harvard CMT solution). Waveforms from NE China event were modeled by WN10, and here for completeness we reiterate the main features of the triplication observed from this event: (1) the AB branch extends to as far as ∼29°; (2) the CD phase does not show up until ∼14°–15° away from the earthquake; (3) the crossover of the AB and CD branches occurs between 19° and 20°.

The second earthquake occurred on July 20, 2008 in the Izu-Bonin arc (Figure 1) with a focal depth of 481 km (USGS PDE catalog) and a moment magnitude of 5.8 (Harvard CMT solution), hereafter we refer to it as the Izu-Bonin event. Seismic waves generated by the Izu-Bonin event were clearly registered by more than 500 broadband stations of the CEArray. The CEArray stations are in the azimuth range of ∼260°–350°. Based on the waveform coherence, we divided the CEArray stations into two azimuthal groups, one in the azimuth range of 260°–297° and the other in 326°–350°. This division is consistent with the focal mechanism of the event, which shows a 313° strike for one of the fault planes (Figure 3). Stations with an azimuth close to 313° were not selected so as to avoid modeling complicated waveforms.

Before fitting the waveform data, we first removed instrumental responses from the data and further filtered the waveform data with a bandpass filter (0.1–1.0 Hz). To represent the data in a comprehensible way, we plotted recording section by aligning the manually picked first arrivals to predictions from certain velocity

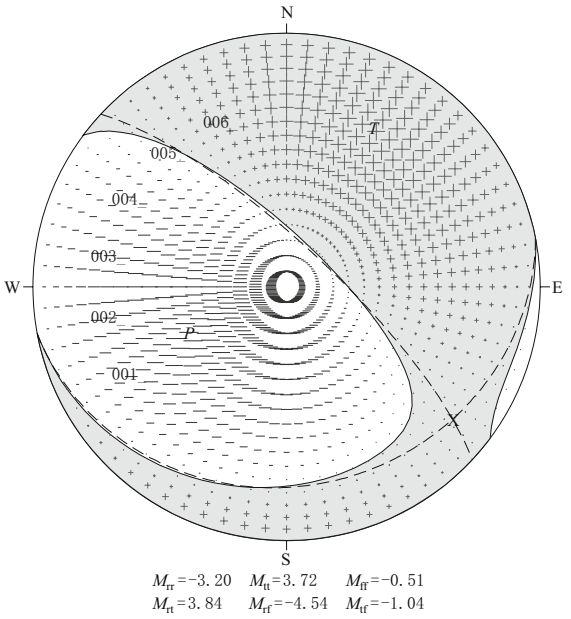

Figure 3 Distribution of normalized amplitudes for the P wave radiated from the Izu-Bonin event are shown as function of takeoff angle and azimuth. "P" and "T" are the compressional and tensional axis. Number 001–006 indicate the azimuths 240°–340°.

model, as done by most 1D forward modeling (e.g., Tajima and Grand, 1998; Wang and Chen, 2009; Wang and Niu, 2010). Figure 4 shows examples of waveforms from the two azimuthal groups. In general, the first recording section (Az 260°–297°) has lower SNR (signal-to-noise ratio) than the second one. We also noticed there is a significant difference in waveform durations. While the waveforms in the second group (Az 326°–350°) have a half duration of ∼2 s, close to the estimate of its CMT solution; those from the first section (Az 260°–297°) are much broader, with a half duration of ∼4 s. A broadened P wave was also observed by Tajima and Nakagawa (2006). Waveforms in the first section also appeared to be less coherent than those in the second group. This is probably due to strong lateral heterogeneity along the ray paths of these low azimuth stations. Since 3D structure may play an important role in generating the complicated waveforms in this group, it may not be appropriate to use 1D or 2D modeling techniques to fit the waveform data. We thus decided to only model the waveform data of the second group (Figure 4b).

Clear triplication can be seen in the recording section and can be summarized as following: (1) the AB phase extends no longer than 23°; (2) the CD has amplitude comparable to the AB from the beginning of the recording section (∼16.5°); (3) the AB and CD braches crossover at around 17.5°. The triplication features shown here is very different from what we observed from the NE China event, they are rather close the global average model, IASP91 (Kennett and Engdahl, 1991).

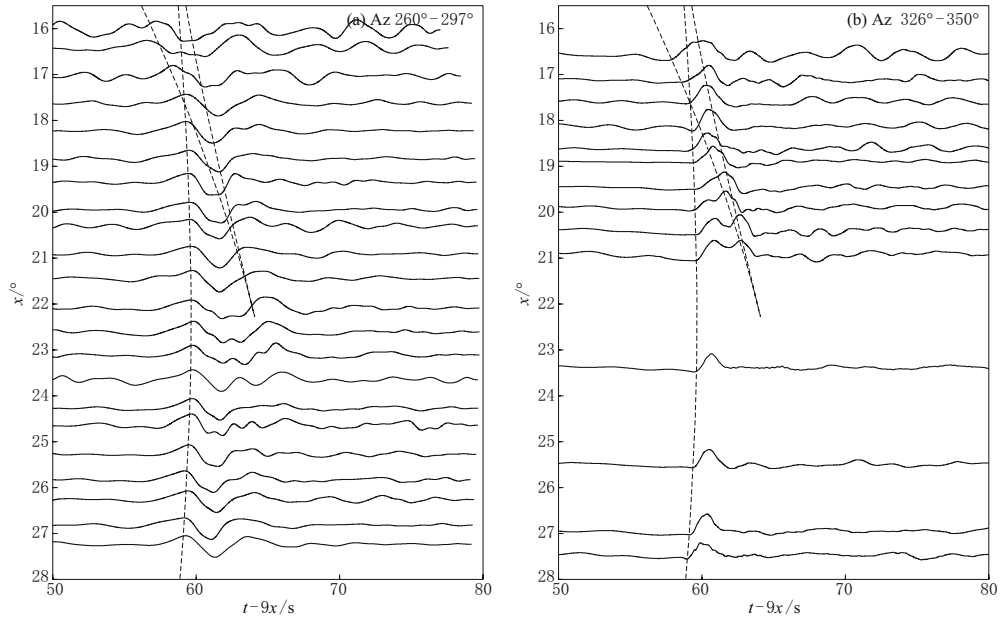

Figure 4 Record sections for the Izu-Bonin event at two different azimuth ranges. For display purpose, only a small portion of the seismograms is shown here. The ray-theory based travel times predicted from IASP91 are plotted in dashed lines. Note here we adjusted the first arrival times of the data in order to align the observed first arrivals with the model predictions. The adjustments are very minor, usually less than 0.7 s.

3 Waveform modeling

In this paper, we follow the analyzing strategy and procedure of WN10. Since uncertainty in earthquake location especially in focal depth may affect the modeling result. We redetermined the focal depth by using the global records of this earthquake (with epicentral distance 30°–90°) collected by the Incorporated Research Institute for Seismology (IRIS). We manually picked the P and pP arrival times from the records and used a grid search method to find the focal depth that minimizes the misfit between observed and IASP91 predicted pP–P differential travel time. As shown in Figure 5, the misfit reaches a minimum at the depth of 481 km, identical to the PDE catalog depth.

Based on the analysis of the NE China event, we found that the maximum reachable distance of the direct AB phase is sensitive to the velocity gradient right above the discontinuity. The minimum distance of the CD phase is closely related to the sharpness and amount of velocity jumps across the discontinuity. Based on the first feature that the extension of the AB phase is comparable to the IASP91 model (Figure 4b), we started with an initial model that has a velocity gradient similar to the IASP91 model for layers above the 660-km. In fitting the data, we did not intend to match the arrival time of the first arrival, but rather emphasized fitting the relative move-out and amplitude of the AB and CD phases. After several iteration of trial and error fitting, we obtained a final 1D velocity that fits the observed waveform data reasonably well (Figure 6). We understand that there are many models that can explain the data within the data uncertainty, and we have chosen a relatively simple model here as the final model. We computed the synthetic seismograms with a modified propagation matrix method proposed by Wang (1999). Synthetics from two rather simple 1D velocity models explain the observed features of the two earthquakes quite well. The time shift between the manually picked and the synthetic first arrivals are usually less than 0.7 s. Some minor misfits can be found at epicentral distances less than 17° for Izu-Bonin event

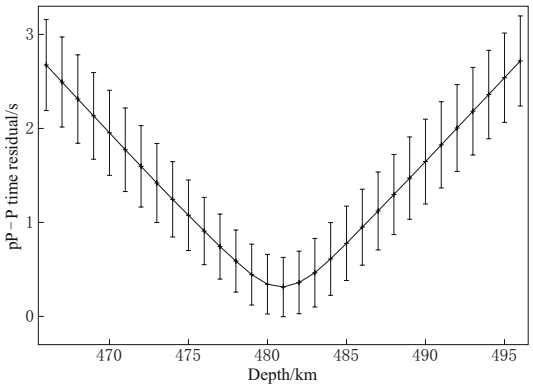

Figure 5 pP–P differential time residuals with respect to the IASP91 model are shown as a function of assumed hypocentral depth.

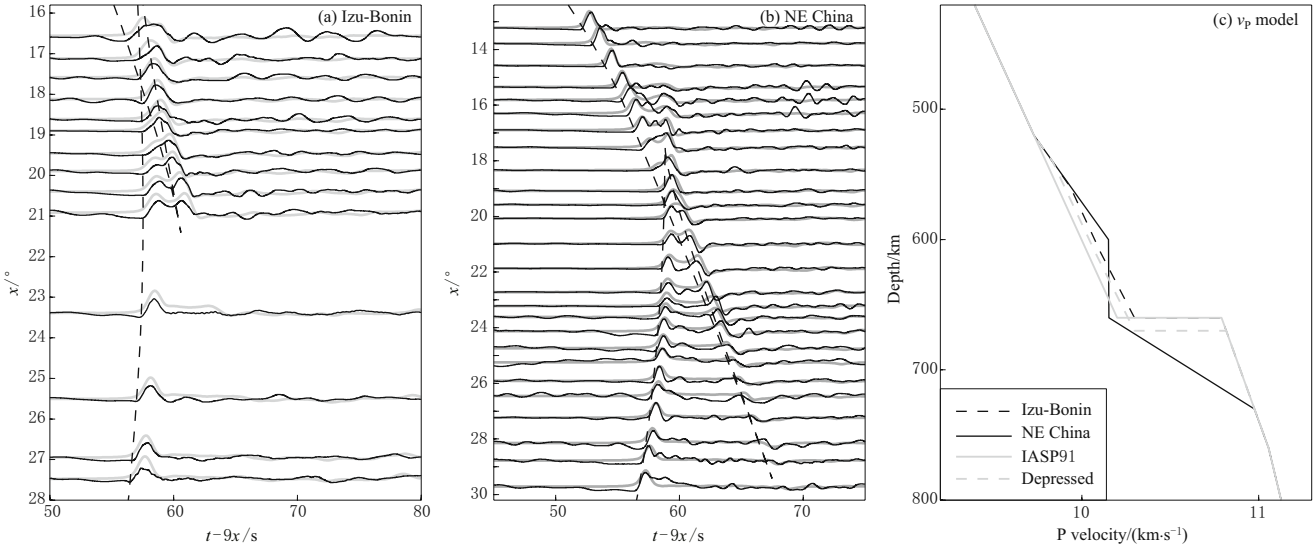

Figure 6 Synthetic waveforms (gray) computed from velocity models for Izu-Bonin event (a) and NE China event (b). (c) Final velocity models for both events are shown together with IASP91 model, also shown is a velocity model with a depressed 660-km discontinuity to 670 km. Observations were aligned with synthetics at the first arrivals. Note the excellent match between the synthetics and the observed waveforms.

and ∼23° for NE China event (Figure 6). So the true models of the two regions must have finer structures than the two relatively simple 1D models shown in Figure 6c. In addition, velocity of the layer immediately below the earthquakes is not well constrained due to limits either in data coverage or in the method. On the other hand, we have very good coverage around the crossover distance of the two phases, so velocity in the layers right above or below the discontinuity is relatively well constrained.

4 Results and discussion

The final velocity models from the those two events show distinct differences (Figure 6c). For the velocity right above the 660-km, the NE China event revealed a layer with an almost constant velocity, i.e. low gradient, while from the Izu-Bonin event we modeled a layer with velocity gradient similar to the IASP91 model. As mentioned above, the gradient is determined from the maximum epicentral distance that the AB phase is able to reach, which is ∼23° and ∼29° for Izu-Bonin event and NE China event, respectively. Records from the NE China event is well explained by a broad (50–70 km) 660-km discontinuity. Models with a velocity jump at the depth of 660 km seem to be able to fit the waveform data of the Izu-Bonin event. On the other hand, velocity increase across the 660-km discontinuity is determined by the differential travel times and the relative amplitudes of the AB and CD phases. As shown in Figure 6, the differential travel times and relative amplitudes are well matched for both events.

Spatial variations of the 660-km discontinuities across various sections of the subduction zones in the western Pacific were studied with a few stations sparsely distributed in China (e.g., Wang et al., 2006; Tajima et al., 2009). As shown in the records of the Izu-Bonin event, waveforms recorded at different azimuths could be very different due to either a difference in radiation pattern or strong lateral heterogeneities. Thus it may be not appropriate to combine records with different azimuths into a single record and model them with a 1D velocity model. With the availability of the CEArray data, we were able to group data within a relatively small azimuthal range. Such grouping can minimize uncertainties induced by unmodeled 3D velocity structure and is obviously more favorable for 1D waveform modeling. With this grouping, we were able to image subtle lateral variations from the NE China event (Wang and Niu, 2010).

A high velocity at transition zone depth is usually interpreted to have a thermal origin associated with subducting slabs. The cold slabs when approaching to the bottom of the upper mantle, can also delay the post-spinel phase change, leading to a depressed 660-km (e.g., Wang et al., 2006; Tajima et al., 2009; Wang and Chen, 2009). From the Izu-Bonin event, we obtained a model with a slightly high velocity above the 660-km

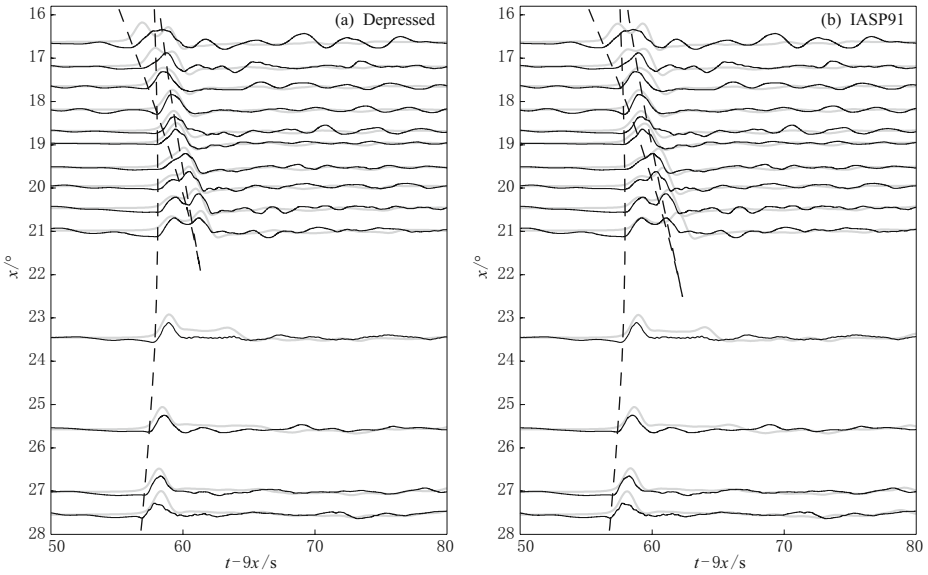

Figure 7 Comparison between observed and synthetic waveforms from the model with a depressed 660-km discontinuity (a) and IASP91 standard model (b).

which shows no depression. We believe both the high velocity and the discontinuity depth are well constrained from the data. For comparison, we calculated synthetics of a 1D model modified from the final Izu-Bonin model. The model has a depressed 660-km at 670 km depth (Figure 6c). Synthetic waveforms corresponding to this model are shown in Figure 7, together with the IASP91 synthetics. The synthetics from the depressed 660-km model showed a poor fit with records before the crossover distance (Figure 7a). On the other hand, the IASP91 synthetics had large misfits with waveforms recorded at large distances (Figure 7b). Tajima et al. (2009) also proposed a similar velocity model (M2.0) with a 660-km discontinuity at its normal depth and

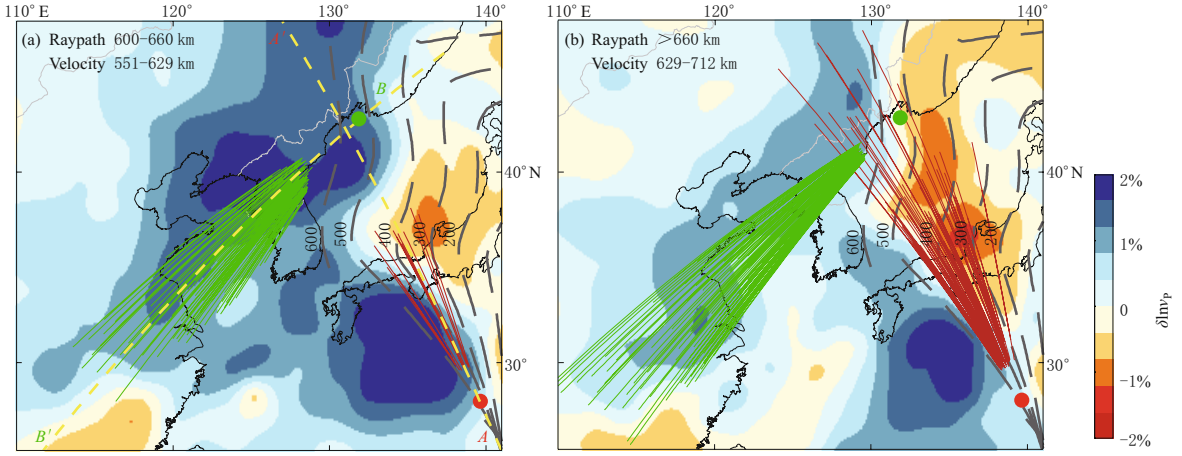

Figure 8 Ray paths for AB (a) and CD (b) branches are plotted on top of tomographic images of Fukao et al. (2001). Ray paths for Izu-Bonin event and NE China event are shown in red and green, respectively. Dots indicate the earthquakes and the dashed gray lines represent the Wadati-Benioff zone of the subducting Pacific slab.

a high velocity above the discontinuity for this region.

The ray paths of the AB and CD arrivals at two depth ranges are shown on top of the tomographic image from Fukao et al. (2001) (Figure 8). Systematic differences can be found for both phases, ray paths from the NE China event fall mainly inside the high velocity regions, while seismic waves from the Izu-Bonin event travels along the northeastern edge of a high velocity body. To further understand the difference shown in the two final 1D models, in Figure 9 we showed two velocity sections along the AA' and BB' lines in Figure 8. We also showed the ray paths of the direct, reflected and refracted waves recorded at 20° (Figure 9). High velocity anomalies beneath Northeast China (Figure 8 and Figure 9b) were interpreted as the subducted Pacific Plate lying above the 660-km discontinuity (Fukao et al., 2001). This high velocity anomaly is well sampled by the AB phase. On the contrary, for the Izu-Bonin event both AB and CD phases only touch the lower boundary of the Pacific Plate (Figure 9a). Little to no anomaly was seen at the turning depths of the two phases, which may explain the normal behavior of the 660-km in this region.

The velocity distributions shown in Figure 9 may be a result of subduction slab geometry. The Pacific

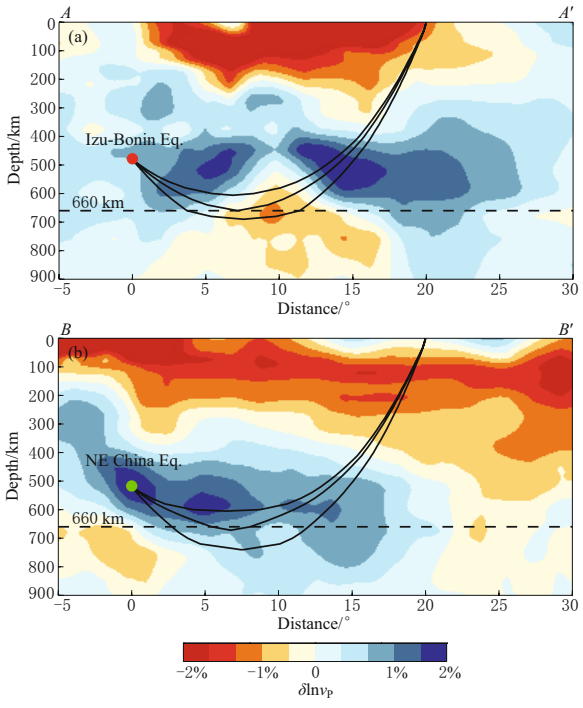

Figure 9 Vertical cross section along AA' and BB' in Figure 8, ray paths for AB, BC, and CD calculated from the corresponding final models (Figure 6c) are shown in solid lines.

Plate is subducting at a high angle beneath Izu-Bonin region. The stations used for Izu-Bonin event are located at the direction almost normal to the westward subducting, and seismic waves recorded by those stations sample the subduction slab before its deflection at the bottom of the upper mantle (Figure 8). In contrast, seismic waves from the NE China event sample mainly the flattened part of the slab. As a result the high velocity anomaly shown in Izu-Bonin region is ∼100 km shallower than that beneath NE China (Figure 9). According to the subduction geometry, we would expect a different structure at lower azimuth ranges in Izu-Bonin region (Tajima et al., 2009) where the Pacific slab may start to lie atop the 660-km discontinuity.

Many studies revealed a depressed 660-km beneath NE China from triplication waveform modeling (e.g., Wang et al., 2006; Tajima et al., 2009; Wang and Chen, 2009). On the other hand, we found that depression is probably the low-resolution image of broadened discontinuity at depth range between 660 km and 720 km. Such a gradual change in velocity is likely caused by a series phase transitions of mantle minerals under low temperature condition (Vacher et al., 1998). We found large variations in the waveform data from the Izu-Bonin earthquake, indicating strong lateral heterogeneities are present near the earthquake source and along the ray paths. Modeling waveform records with high azimuthal angles and raypaths sampling the lower boundary of the Pacific slab results in a relatively "normal" velocity structure located northeast to the Izu-Bonin arc.

5 Conclusions

We investigated spatial variations of velocity structure around the 660-km discontinuity in western Pacific subduction based on used triplication data recorded by CEArray from two deep focus earthquakes. The high station density of the CEArray allowed us to use stations within a narrow azimuth to better constrain 1D velocity structures. We found a very broad 660-km beneath NE China and relatively normal mantle below the Pacific Plate in the northeast flank of the Izu-Bonin arc. The difference in the P-wave velocity structure seems to be caused mainly by the temperature anomalies posted by the subducting Pacific Plate. Further studies with more events and on the S-wave velocity structure around the 660-km discontinuity will certainly help to clarify this interpretation.

Acknowledgements Waveform data for this study were provided by Data Management Centre of the China National Seismic Network at Institute of Geophysics, China Earthquake Administration. We thank Prof. Rongjiang Wang for making his code available to us. Critical comments from two anonymous reviewers significantly improved the quality of this paper. This work was supported by National Natural Science Foundation of China under grant 40874095 and NSF under grant EAR-063566.

References

Ai Y, Zheng T, Xu W, He Y and Dong D (2003). A complex 660 km discontinuity beneath northeast China. *Earth Planet Sci Lett* **212**: 63–71.

Andrews J and Deuss A (2008). Detailed nature of the 660 km region of the mantle from global receiver function data. *J Geophys Res* **113**: B06304, doi:10.1029/2007JB005111.

Brudzinski M R and Chen W P (2003). A petrologic anomaly accompanying outboard earthquakes beneath Fiji-Tonga: Corresponding evidence from broadband P and S waveforms. *J Geophys Res* **108**, doi:1029/2002JB002012.

Fukao Y, Widiyantoro S and Obayashi M (2001). Stagnant slabs in the upper and lower mantle transition region. *Rev Geophys* **39**: 291–323.

Ito E and Takahashi E (1989). Postspinel transformations in the system Mg_2SiO_4-Fe_2SiO_4 and some geophysical implications. *J Geophys Res* **94**: 10 637–10 646.

Kennett B L N and Engdahl E R (1991). Traveltimes for global earthquake location and phase identification. *Geophys J Int* **105**: 429–465, doi:10.1111/j.1365-246X.1991.tb06724.x.

Nakajima J and Hasegawa A (2007). Subduction of the Philippine Sea plate beneath southwestern Japan: Slab geometry and its relationship to arc magmatism. *J Geophys Res* **112**: B08306, doi:10.1029/2006JB004770.

Niu F and Kawakatsu H (1996). Complex structure of mantle discontinuities at the tip of the subducting slab beneath Northeast China—A preliminary investigation of broadband receiver functions. *J Phys Earth* **44**: 701–711.

Niu F, Levander A, Ham S and Obayashi M (2005). Mapping the subducting Pacific slab beneath southwest Japan with Hi-net receiver functions. *Earth Planet Sci Lett* **239**: 9–17.

Shearer P M and Masters T G (1992). Global mapping of topography on the 660-km discontinuity. *Nature* **355**: 791–796.

Tackley P J (2008). Layer cake or plum pudding? *Nature Geoscience* **1**: 157–158.

Tajima F and Grand S P (1998). Variation of transition zone high-velocity anomalies and depression of 660 km discontinuity associated with subduction zones from the southern Kuriles to Izu-Bonin and Ryukyu. *J Geophys Res* **103**: 15 015–15 036.

Tajima F and Nakagawa T (2006). Implications of seismic waveforms: Complex physical properties associated with stagnant slab. *Geophys Res Lett* **33**: L03311, doi: 10.1029/2005GL024314.

Tajima F, Katayama I and Nakagawa T (2009). Variable seismic structure near the 660 km discontinuity associated with stagnant slabs and geochemical implications. *Phys Earth Planet Inter* **172**: 183–198.

Vacher P, Mocquet A and Sotin C (1998). Computation of seismic profiles from mineral physics: the importance of the non-olivine components for explaining the 660 km depth discontinuity. *Phys Earth Planet Inter* **106**: 275–298.

Vidale J and Benz H (1992). Upper-mantle seismic discontinuities and the thermal structure of subduction zones. *Nature* **356**: 678–680.

Wang B and Niu F (2010). A broad 660-km discontinuity beneath northeast China revealed by dense regional seismic networks in China. *J Geophys Res* **115**: B06308, doi:10.1029/2009JB006608.

Wang R (1999). A simple orthonormalization method for stable and efficient computation of Green's functions. *Bull Seismol Soc Am* **89**: 733–741.

Wang T and Chen L (2009). Distinct velocity variations around the base of the upper mantle beneath northeast Asia. *Phys Earth Planet Inter* **172**: 241–256.

Wang Y, Wen L, Weidner D and He Y (2006). SH velocity and compositional models near the 660-km discontinuity beneath South America and northeast Asia. *J Geophys Res* **111**: B07305, doi:10.1029/2005JB03849.

Zheng X F, Ouyang B, Zhang D N, Yao Z X, Liang J H and Zheng J (2009). Technical system construction of Data Backup Centre for China Seismograph Network and the data support to researches on the Wenchuan earthquake. *Chinese J Geophys* **52**: 1 412–1 417, doi: 10.3969/j.issn.0001-5733 (in Chinese).